Research article

IN BIOMEDICINE

Received: 25 April 2015, Revised: 27 April 2016, Accepted: 30 April 2016, Published online in Wiley Online Library: 24 August 2016

(wileyonlinelibrary.com) DOI: 10.1002/nbm.3565

Characterization of a novel MR-detectable nanoantioxidant that mitigates the recall immune response

Taeko Inoue[a†], Deric M. Griffin[c†], Redwan Huq[a], Errol L. G. Samuel[b], Simone H. Ruano[a], Gary Stinnett[a], Tabassum J. Majid[c], Christine Beeton[a,c], James M. Tour[b]* and Robia G. Pautler[a,c]*

In many human diseases, the presence of inflammation is associated with an increase in the level of reactive oxygen species (ROS). The resulting state of oxidative stress is highly detrimental and can initiate a cascade of events that ultimately lead to cell death. Thus, many therapeutic attempts have been focused on either modulating the immune system to lower inflammation or reducing the damaging caused by ROS. Berlin *et al*. reported the development of a novel nanoantioxidant known as poly(ethylene glycol)-functionalized-hydrophilic carbon clusters (PEG-HCCs). They showed that PEG-HCCs could be targeted to cancer cells, utilized as a drug delivery vector, and can even be visualized *ex vivo*. Our work here furthers this work and characterizes Gd-DTPA conjugated PEG-HCCs and explores the potential for *in vivo* tracking of T cells in live mice. We utilized a mouse model of delayed-type hypersensitivity (DTH) to assess the immunomodulatory effects of PEG-HCCs. The T_1-agent Gd-DTPA was then conjugated to the PEG-HCCs and T_1 measurements, and T_1-weighted MRI of the modified PEG-HCCs was done to assess their relaxivity. We then assessed if PEG-HCCs could be visualized both *ex vivo* and *in vivo* within the mouse lymph node and spleen. Mice treated with PEG-HCCs showed significant improvements in the DTH assay as compared to the vehicle (saline)-treated control. Flow cytometry demonstrated that splenic T cells are capable of internalizing PEG-HCCs whereas fluorescent immunohistochemistry showed that PEG-HCCs are detectable within the cortex of lymph nodes. Finally, our nanoantioxidants can be visualized *in vivo* within the lymph nodes and spleen of a mouse after addition of the Gd-DTPA. PEG-HCCs are internalized by T cells in the spleen and can reduce inflammation by suppression of a recall immune response. PEG-HCCs can be modified to allow for both *in vitro* and *in vivo* visualization using MRI.

Keywords: MRI; nanotechnology; oxidative stress; cell labeling; T1 agents; PEG-HCCs; antioxidant; inflammation

INTRODUCTION

A multitude of human diseases including diabetes, cancers and neurogenerative diseases are associated with inflammation and increased production of free radicals resulting in a state of oxidative stress (1–4). These hallmarks of inflammation and ROS elevation have been shown to cause damage to tissues and organs by damaging organelles and cell components such as mitochondria, DNA, lipids and proteins (5–7). Once this cascade of events has been initiated, the result is typically apoptosis and in the case of neurodegenerative disease, the loss of irreplaceable neurons (1–4,6,7). As a result, much time and research have been spent studying how to mitigate inflammation and oxidative stress using immunomodulatory drugs and antioxidants, respectively.

* *Correspondence to: Robia G. Pautler, Department of Molecular Physiology & Biophysics, Baylor College of Medicine, One Baylor Plaza, Houston, TX 77030, USA. E-mail: rpautler@bcm.edu*
James M. Tour, Ph.D. T. T. and W. F. Chao Professor of Chemistry Professor of Computer Science Professor of Materials Science and NanoEngineering Rice University NanoCarbon Center, Houston, Texas. E-mail: tour@rice.edu

a *T. Inoue, R. Huq, S. H. Ruano, G. Stinnett, C. Beeton, R. G. Pautler*
Department of Molecular Physiology & Biophysics, Baylor College of Medicine, Houston, TX, USA

b *E. L. G. Samuel, J. M. Tour*
Department of Chemistry, Department of Material Science and NanoEngineering and The NanoCarbon Center, Rice University, Houston, Texas, USA

c *D. M. Griffin, T. J. Majid, C. Beeton, R. G. Pautler*
Interdepartmental Program in Translational Biology & Molecular Medicine, Baylor College of Medicine, Houston, TX, USA

† *These two authors contributed equally to the work.*

Abbreviations used: *ANOVA, analysis of variance; BSA, bovine serum albumin; DTH, delayed-type hypersensitivity; DPBS, Dulbecco's phosphate-buffered saline; EDTA, ethylenediaminetetraacetic acid; FOV, field of view; Gd-DTPA, gadolinium diethylene pentaacetic acid; MRI, magnetic resonance imaging; PEG-HCC, poly(ethylene glycol)-functionalized-hydrophilic carbon clusters; PFPE, perfluoropolyether; RARE, rapid acquisition with refocused echoes; ROS, reactive oxygen species; SPIO, super paramagnetic iron oxide; VTR, variable T1 relaxation.*

The novel nanoantioxidants used within this study are poly(ethylene glycol)-functionalized-hydrophilic carbon clusters (PEG-HCCs) (8,9). PEG-HCCs were first developed and described by Lucente-Schultz *et al.* 2009 and are derived from ultra-short, single-walled carbon nanotubes that are heavily oxidized, water soluble and approximately 40 nm in length and 2–3 nm wide. PEG moieties are added to their sidewalls for improved biodistribution. Berlin *et al.* (10) then demonstrated the flexibility of these nanoantioxidants in that their side walls could be non-covalently functionalized with antibodies and also demonstrated their effectiveness as an *in vitro* antioxidant (10). Their work showed that PEG-HCCs were highly effective at scavenging oxygen radicals, more so than trolox, a vitamin E analog (8). They have been utilized *in vivo*, within a rat model of traumatic brain injury (TBI), where Bitner *et al.* showed that PEG-HCCs improve cerebral blood flow post-TBI via the scavenging of superoxide molecules (9). Finally, aside from their antioxidant capacity, PEG-HCCs have also been utilized as a targeted vector for the transport of paclitaxel, an anti-cancer medication, to tumor cells by the non-covalent addition of antibodies to their side-walls (10). Most striking of all in these studies is the lack of toxicity in cells, mice or rats. This exquisite safety profile is probably as a result of their ultra-short, ultra-small size (approximately the size of proteins), a high degree of oxidation, undetectable metal content, water solubility, high dispersion and low aggregation owing to PEGylation (10).

The field of cell labeling, specifically of T cell labeling, has worked towards developing an agent that will allow the longitudinal tracking of T cells in an *in vivo* system using MRI. Thus far, studies have shown that T cells can be labeled *in vitro* with several agents such as superparamagnetic iron oxide particles (SPIOs) or a novel perfluoropolyether (PFPE) nanoparticle (11–13). As signal intensity is dependent on the levels of loading within the cells, they must be loaded *in vitro* to ensure high levels of loading. Labeled cells are then adoptively transferred into the animal for imaging. Unsurprisingly, there are some drawbacks to these methods. In both cases, there are biocompatibility concerns. In the case of the SPIOs, there is difficulty distinguishing the signal from background and artifacts due to the T_2* nature of SPIO imaging (12,13). In the case of PFPE, the signal intensity is low, even when cells are pre-loaded with the agents and adoptively transferred. There is also a loss of signal as cells divide (11,14). Finally, there is still limited uptake by T cells versus uptake by monocytes, which is speculated to be because of the smaller size and lower phagocytic function of T cells compared with that of monocytes (11–14). Thus, there is still a need for a T cell-specific labeling agent that has a high signal, i.e. T_1-agent.

As we worked to characterize the PEG-HCCs, we discovered that upon subcutaneous administration of our nanoantioxidants, they localized within the draining lymph nodes in a reproducible and very specific pattern. This pattern coincided with the cortex of the lymph nodes. Consequently, we became interested in verifying whether the PEG-HCCs were localizing within T cells and could be utilized as a T cell labeling agent. To assess the ability of PEG-HCCs to affect T cells, we first used a mouse model of delayed-type hypersensitivity (DTH). DTH is an inflammatory response mediated by T cells and antigen-presenting cells such as macrophages or dendritic cells. The recall immune reaction observed during DTH is similar to that leading to pancreatic beta cell death in type-1-diabetes and demyelination in multiple sclerosis.

This study adds a number of new and important characteristics to the lengthening list of PEG-HCC functions in that they (i) suppress the recall immune response *in vivo*, (ii) enter the cortex of lymph nodes and the spleen, (iii) are internalized by splenic T cells and (iv) can be modified with the addition of gadolinium complexed to diethylene triamine pentaacetic acid ([Gd]DTPA) for *in vivo* visualization utilizing MRI. We report our findings of treating mice with PEG-HCCs and make new observations as to their localization within immune organs, i.e. lymph node and spleen both *in vivo* and *ex vivo*. Our findings not only indicate that these nanoantioxidants can modulate the immune system but also can be monitored both *ex vivo* and *in vivo* via the addition of an MR-detectable moiety.

METHODS

Preparation of PEG-HCCs and [Gd]DTPA-PEG-HCCS

DTPA-PEG-HCCs, prepared as previously described by Berlin *et al.* 2010 (10), were placed in a vial (5 mL, 314 mg/L HCC core). An aqueous solution of $GdCl_3$•6 H_2O (Sigma-Aldrich (St. Louis, MO, USA), 12 mg in 100 μL DI H_2O) was added to this vial. The solution was then vortexed for 5 min then allowed to stand for 30 min before it was passed through a PD-10 column to remove excess Gd^{3+}.

Mice

All mice utilized for this work were C57Bl/6 J (Jackson Laboratory Bar Harbor, ME, USA) approximately 10–15 weeks of age. Animal housing and handling were in compliance with NIH Guidelines for the Care and Use Laboratory Animals. Animal protocols were approved by The Institutional Animal Care and Use Committee (IACUC) at Baylor College of Medicine before any work was carried out.

Mouse treatment paradigm and lymph node and spleen collection

All mice were treated under anesthesia, i.e. 5% isoflurane and 100% oxygen. For lymph node imaging, C57Bl/6 J mice were given subcutaneous injections near the base of the tail of 200 μL of PEG-HCC (300 g/L), [Gd]DTPA-PEG-HCC (300 mg/L), 5 mM Magnevist® (Bayer HealthCare, Wayne, NJ, USA) or vehicle (saline Butler Schein, Dublin, OH, USA) near the base of the tail. For spleen MR and flow cytometry experiments, mice were, respectively, given scapular subcutaneous injections of 200 μL of [Gd]DTPA-PEG-HCCs (200 mg/L), PEG-HCC (200 mg/L) or the vehicle. Twenty-four hours post-injection, mice were anesthetized using 5% isoflurane and oxygen and sacrificed using cervical dislocation. Inguinal and axillary lymph nodes were then removed and either embedded in 1% agarose for MR imaging or placed in 10% formalin for histology. The spleens were also harvested 24 h post-injection and prepared for flow cytometry. For spleen MR experiments, mice were sacrificed as above, and the spleens were imaged in the intact mouse.

Flow Cytometry

Spleens harvested from mice were placed in ice-cold calcium and magnesium free 1X Dulbecco's phosphate-buffered saline (DPBS Cellgro, Manassas, VA, USA). A single-cell suspension of splenocytes was created of the spleen in 15 mL of 1X DPBS and straining the mixture through a 70-μm cell strainer. Cells were then counted using a hemacytometer and a total of 2.5 x 10^5 cells were used for each experimental condition. Experimental conditions were as follows: samples from PEG-HCC and vehicle-treated animals were either kept intact during wash and incubation steps, using a buffer composed of 1X DPBS with 2% goat serum and 2% bovine serum

albumin (BSA Santa Cruz Biotechnology, Dallas, TX, USA) or permeabilized using the previously indicated buffer with the addition of 0.5% saponin (Sigma-Aldrich, St. Louis, MO, USA).

After counting, cells were stained with a primary rabbit antibody against PEG (Abcam ab51257 Cambridge, MA, USA) at 1:803 in addition to a primary antibody against CD3 conjugated to allophycocyanin (APC; Ebioscience 17–0032 San Diego, CA, USA) at 1:80. Cells were then washed in their respective buffers and stained with an anti-rabbit Alexa Fluor 488 antibody (Life Technologies A11034 Carlsbad, CA, USA) and washed again. After washing, cells were fixed in ice-cold 1X DPBS with 1% paraformaldehyde and stored at 4 °C until data acquisition.

Data were acquired on a Becton Dickinson Canto II cell analyzer. Compensation controls included unstained intact cells, intact cells incubated with Alexa Fluor 488-conjugated CD45R (Invitrogen RM2620 Carlsbad, CA, USA), and intact cell incubated with an APC-conjugated CD3 antibody. Intact and permeabilized samples incubated with APC-conjugated CD3 and Alexa Fluor 488 secondary served as controls to remove the background PEG signal.

Data were analyzed using FloJo (Treestar) and statistical analysis was performed with a two-way ANOVA with a Tukey multiple comparisons test.

Histology

To assess the localization of [GD]DTPA-PEG-HCCs within lymph nodes, we carried out immunohistochemistry of lymph node collected [Gd]DTPA-PEG-HCC and vehicle-treated mice. Lymph nodes were placed in 10% buffered formalin immediately after collection and embedded in paraffin for sectioning. Lymph node sections were deparaffinized and rehydrated using the following gradient: 100% xylene (3X 3 min), 1:1 (v/v) ratio of 100% ethanol to 100% xylene (1X 3 min), 100% ethanol (1X 3 min), 95% ethanol (1X 3 min), 80% ethanol (1X 3 min), 70% ethanol (1X 3 min) and deionized tap water (2X 3 min). Heat-mediated antigen retrieval was then performed by microwave heating slides in a Tris-EDTA buffer for 20 min after which sections were blocked for 2 h at room temperature in a solution of 1X Tris-buffered saline (TBS) with 1% BSA and 10% normal goat serum. After blocking, slides were then incubated with blocking buffer (1% BSA in TBS) containing primary antibodies against the T-cell surface marker CD3 (Abcam ab11089 Cambridge, MA, USA) and PEG (Abcam ab51257 Cambridge, MA, USA) at 1:100 overnight at 4 °C in a humidified box. Slides were then washed in 1X TBS twice for 5 min each, then were incubated with blocking buffer containing anti-rat Alexa Fluor 488 (Abcam ab150157 Cambridge, MA, USA) and anti-rabbit Alexa Fluor 568 (Abcam ab175471 Cambridge, MA, USA) at 1:100 for 1 h at room temperature. Slides were then washed (3X 5 min) in TBS, dried and mounted with media containing DAPI. Finally, images were taken using an Olympus 1X71 microscope (Tokyo, Japan).

Delayed-type hypersensitivity (DTH) induction and monitoring

Active DTH was carried out as previously described by Beeton *et al.* (15). Briefly, 10-week-old, female C57Bl/6 J mice were immunized against ovalbumin (OVA) using an emulsion consisting of a 1:1 ratio of Complete Freund's Adjuvant (Difco, Sparks, MD, USA) and OVA (Sigma-Aldrich, St. Louis, MO, USA). Each mouse received100 μL emulsion at the base of the tail (100 μg OVA/mouse). Before immunization, mice were treated intravenously with 100 μl of PEG-HCCs (300 mg/L) or vehicle once a week for 5 weeks. One week after immunization, mice were challenged with 10 μL of a 2 mg/mL solution of OVA in the pinna of one ear and a solution of the vehicle in the other. One day after challenge, the ear thickness was measured using a spring-loaded micrometer and the difference in size between the vehicle-treated ear and the OVA-treated ear was used as a measure of inflammation. Data from DTH assay were analyzed by one-way ANOVA with Tukey's multiple comparisons test (GraphPad Prism La Jolla, CA, USA).

Ex Vivo and In vivo MRI

We assessed whether [GD]DTPA-PEG-HCCs could be visualized using T_1-weighted MR scans within a mouse lymph node and spleen both *ex vivo* and *in vivo*. Mice were treated with 100 μL of 200 mg/L concentration PEG-HCC, [Gd]DTPA-PEG-HCC, 5 mM Magnevist® or vehicle as described previously. Twenty-four hours post-injection, mice were anesthetized with 5% isoflurane and 100% oxygen, placed in the animal holder (Bruker BioSpin, Billerica, MA, USA) and kept under 2% isoflurane and oxygen and imaged using 9.4 T, Bruker Avance BioSpec Spectrometer with a 21-cm horizontal bore (Bruker BioSpin Billerica, MA, USA) and a 35-mm resonator. During imaging, breathing was monitored, and the body temperature was kept at 37 °C using an animal heating system (SA Instruments, Stony Brook, NY, USA). After imaging, mice were removed from the MRI and placed on a heating pad until they woke up, after which they were placed back into their cages.

Protocol for MR scans

Mice were imaged using a Rapid Acquisition with Refocused Echoes (RARE) protocol to obtain T_1-weighted images with the following parameters: TE = 11.72 ms, TR = 590.94 ms, FOV = 25 mm, matrix size =256 x 256, taking 2 min, 31 s and 280 ms. T_1-measurements were done using a RARE protocol with a Variable Acquisition Time (RAREVTR) as described by (16) with the following parameters: TE = 10 ms, TR = 200–6000 ms, FOV = 20 mm, matrix size =128 x 128, taking 4 min, 3 s and 200 ms. *Ex vivo* and *in vivo* scans were carried out using a RARE protocol with the following parameters: TE = 7.51 ms, TR = 1500 ms, average = 4, rare factor = 4, FOV = 36 x 30 mm, matrix size =256 x 256, each taking 4 min and 48 s. All scans were carried out using Paravision 4.0 software (Bruker BioSpin Billerica, MA, USA).

T_1 maps were acquired using an RARE-VTR sequence with TRs = 29.447, 632.50, 1656.89 and 7500 ms. TE = 6.567 ms and RARE factory =2. FOV = 4 x 4 cm, matrix =128 x 128, number of slices =1 and slice thickness = 1.5 mm. T_1-maps were made using PV5.1.

RESULTS

PEG-HCCs can function as immunomodulators

Previous work has shown that PEG-HCCs can scavenge radicals and lower ROS levels *in vivo* after traumatic brain injury (8,9). However, no data has been shown on their immunomodulatory characteristics. We chronically treated C57Bl/6 J mice with PEG-HCCs or vehicle once a week over a 5-week period. At week 4, we carried out a DTH assay, which assesses the recall immune response to a specific antigen; OVA was used here. We found that chronic treatment with PEG-HCCs resulted in decreased inflammation when compared to saline-treated mice as shown in Fig. 1. Our results demonstrate that chronic treatment with PEG-HCCs once a week, for five total treatments, have immunomodulatory effects by reducing an antigen-specific recall response in an *in vivo* system.

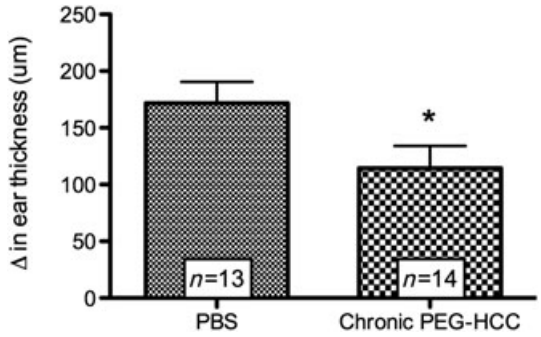

Figure 1. PEG-HCCs are immunomodulating. C57Bl/6 J mice were treated chronically for a period of 5 weeks with either PEG-HCC or vehicle. Ear swelling after OVA challenge shows that chronic treatment with PEG-HCCs resulted in significantly reduced inflammation compared to those treated with vehicle. $*p < 0.05$.

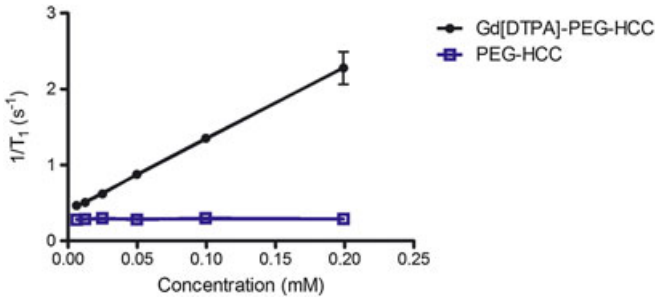

Figure 3. [Gd]DTPA-PEG-HCCs have increased relaxivity compared to PEG-HCC alone. Relaxivity was measured using two different batches of [Gd]DTPA-PEG-HCC. There was little variation to be seen within the two samples, and the relaxivity was measured to be approximately $9.5\ mM^{-1}\ s^{-1}$ with a correlation coefficient of 0.9895. PEG-HCC alone, however, did not show any concentration dependent changes in T_1-times.

Addition of Gadolinium changes the T_1-properties of PEG-HCCs

For *in vivo* imaging, we utilized gadolinium along with the PEG-HCCs, to generate [Gd]DTPA-PEG-HCCs. Using a T_1-weighted protocol, we were able to show that [Gd]DTPA-PEG-HCCs (tube 2) at 340 mg/L had increased signal intensity as shown in Fig. 2 compared to a solution of PEG-HCCs alone (tube 1) at 690 mg/L. The measurement of T_1-times shows that addition of the gadolinium moiety results in significantly lower T_1-times for the [Gd]DTPA-PEG-HCCs compared to PEG-HCC alone as shown in the graphs in Fig. 2. Our next step was to measure the relaxivity of the [Gd]DTPA-PEG-HCCs. At 9.4 T, the relaxivity of [Gd]DTPA has been reported to be approximately $3.9\ s^{-1}\ mmol^{-1}$. We first measured the relaxivity of PEG-HCCs alone and observed that there is no concentration-dependent change in T_1-time as shown in the line graph in Fig. 3. With the addition of [Gd]DTPA to the PEG-HCCs, however, we see a change in the T_1-time that correlates with the concentration of the [Gd]DTPA-PEG-HCC solution. The slope of this line is $9.5\ mM^{-1}\ s^{-1}$ indicating the possibility of 2–3-[Gd]DTPA moieties on each of the PEG-HCC molecules.

Our results demonstrate our ability to modify the PEG-HCCs into T_1-contrast agents and the potential of our [Gd]DTPA-PEG-HCCs as MR-detectable agents, giving us a way to assess their delivery and localization to biologically relevant locations.

Treatment with [Gd]DTPA-PEG-HCCs results in accumulation in lymph nodes

It was previously shown that PEG-HCCs are rapidly cleared from the body of mice. However, there is some initial accumulation in the liver and spleen, but the lymph nodes were not investigated. In fact, it has been shown that PEG-HCCs and similar particles are cleared via the biliary pathway, and as expected, this results in accumulate in the liver (10). The spleen is also highly vascularized which allows for the accumulation within the spleen. Interestingly, we discovered that the administration of PEG-HCCs and [Gd]DTPA-PEG-HCCs, subcutaneously at the base of the tail of mice, resulted in the high accumulation of [Gd]DTPA-PEG-HCCs within the draining lymph nodes 24-h post-injection. This can be seen in Fig. 4 where the accumulation of the [Gd]DTPA-PEG-HCCs forms a distinctive black patterning within the lymph node (see inset).

Ex vivo imaging of treated lymph nodes shows positive contrast

Twenty-four hours after mice were injected subcutaneously at the base of the tail with [Gd]DTPA-PEG-HCCs, their auxiliary lymph nodes were carefully excised from the fat pad and embedded into 1% agarose for imaging via MRI. [Gd]DTPA-PEG-

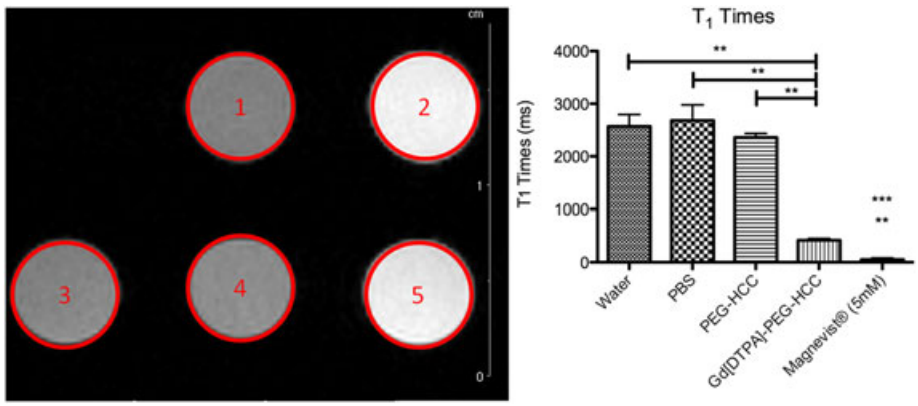

Figure 2. [Gd]DTPA-PEG-HCCs have increased signal intensity compared to PEG-HCCs alone. T_1-weighted scans and T_1-times of [Gd]DTPA-PEG-HCCs, PEG-HCCs and appropriate controls were assessed in 0.2-mL tubes at room temperature. The signal intensity of phantoms containing [Gd]DTPA-PEG-HCC is comparable to that of Magnavist® compared to that of phosphate-buffered (PBS), water or PEG-HCC alone. T_1-times were also measured, and the T_1-times of [Gd]DTPA-PEG-HCC is also decreased compared to PEG-HCC alone. 1-PEG-HCC, 2-[Gd]DTPA-PEG-HCC, 3-Water, 4-PBS, 5-Magnevist (5 mM). $**p < 0.01$, $***p < 0.001$.

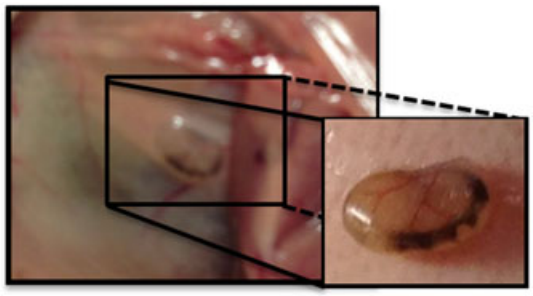

Figure 4. [Gd]DTPA-PEG-HCCs accumulate in draining lymph nodes. Twenty-four hours post-injection, [Gd]DTPA-PEG-HCCs can be seen visually to accumulate in the draining lymph nodes (axiliary lymph nodes) after subcutaneous injection at the base of the tail in C57Bl/6 J mice.

HCC overnight imaging utilizing a T_1-weighted scan showed an increase in signal intensity along the same zones where [Gd]DTPA-PEG-HCC accumulation was visualized as seen in Fig. 5. We do not see this increase in signal intensity in the lymph nodes from mice treated with vehicle indicating that the change in signal intensity is as a result of accumulation of [Gd]DTPA-PEG-HCCs.

In vivo imaging of treated mice shows positive contrast in lymph nodes

We have seen that the [Gd]DTPA-PEG-HCCs can be visualized *in vitro* within phantoms, *ex vivo* within lymph nodes after careful removal of the surrounding fat tissue. We then sought to visualize them *in vivo* within the lymph nodes of C57Bl/6 J mice. We were able to select a single slice through the center of the lymph node. A band of increased signal intensity can be seen along the edge of the lymph node similar to what was seen in the excised lymph nodes, which we do not see in the lymph node of a mouse treated with vehicle as shown in Fig. 6. Images were normalized to a water phantom that was included in all imaging, and the application of a Gaussian filter was used to enhance this bright band seen in the [Gd]DTPA-PEG-HCC-treated lymph node in Fig. 6. A plot graph of a line through each of the lymph nodes shows the increased signal intensity along the edge of the lymph node that we do not see in the vehicle-treated one in Fig. 7.

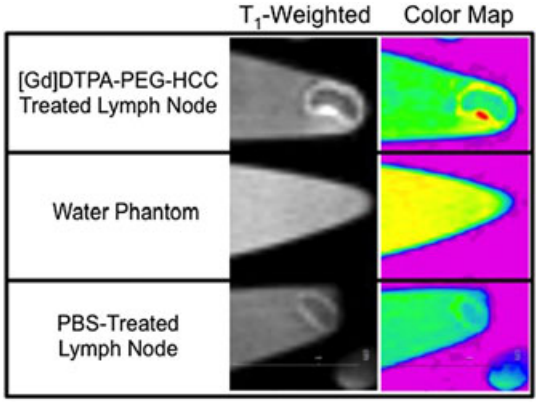

Figure 5. [Gd]DTPA-PEG-HCC-treated lymph nodes can be visualized *ex vivo* with MRI. Lymph nodes were embedded in 1% agarose and were imaged using T_1-weighted MRI. Shown above are the [Gd]DTPA-PEG-HCC treated lymph node (top), vehicle-treated lymph node (bottom), which were both embedded in 1% agarose, and water in a PCR tube (middle). The first column of images demonstrate that the [Gd]DTPA-PEG-HCC treated lymph node shows increased T_1-signal intensity along where there is accumulation of [Gd]DTPA-PEG-HCC, while this increase in signal is not observed in the vehicle-treated lymph node. This signal intensity increase is further demonstrated with the application of a color map (second column) has been applied to indicate increased levels of signal intensity. The hotter (red) colors indicate higher T_1-signal intensity, wherea colder colors (blue) indicate a lower T_1-signal intensity.

[Gd]DTPA-PEG-HCCs can be detected around germinal centers of lymph nodes

We have shown that PEG-HCCs are immunomodulatory in that they suppress an immune recall response to a specific antigen, OVA, as shown by the DTH assay. Also, the [Gd]DTPA-PEG-HCCs appear not to be present throughout the lymph nodes but rather to localize a specific zone. As a result, we decided to carry out immunofluorescence staining for CD3, a T cell marker, and PEG for the [Gd]DTPA-PEG-HCCs. Any co-localization of these antibodies would indicate that our [Gd]DTPA-PEG-HCCs are being taken up by T cells, which would be a novel finding on its own as T cell labeling with a T_1 contrast agent has yet to be reported.

As seen in Fig 8, the [Gd]DTPA-PEG-HCCs localize in the cortex around germinal centers within the lymph nodes. Although the lymph node section taken from the vehicle-treated mouse did not show any positive signal for PEG, as shown in Fig. 8b, a signal was detected in the lymph nodes of [Gd]DTPA-PEG-HCCs-treated mice, in an area outside the T cell zone suggesting the presence of the nanomaterials in the lymphatics within draining lymph nodes. A cartoon of the lymph node anatomy is shown in Fig. 8c.

We then assessed what happens to the T_1 in the spleen after treatment with [Gd]DTPA-PEG-HCCs. We determined using T_1 mapping that there is a decrease in the T_1 values in the spleen of animals treated with [Gd]DTPA-PEG-HCCs compared to animals treated with saline (Fig. 9). The T_1 maps of the spleen in mice that were treated with [Gd]DTPA-PEG-HCCs were not uniform indicating that only certain parts of the spleen were accumulating the [Gd]DTPA-PEG-HCCs. Histograms of the T_1 maps within the spleen demonstrate a clear shift to lower T_1 values in spleens treated with Gd]DTPA-PEG-HCCs compared with vehicle (Fig. 9).

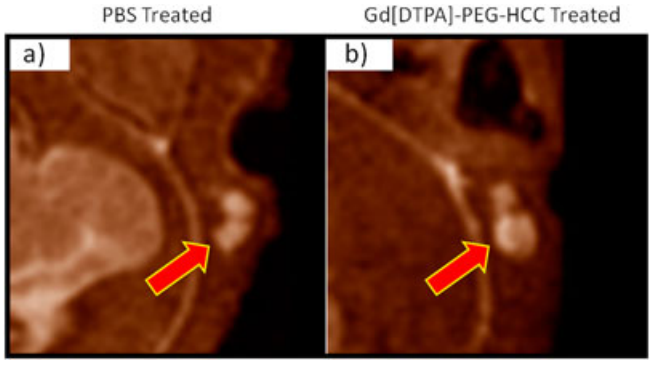

Figure 6. [Gd]DTPA-PEG-HCC accumulation can be seen in lymph nodes. [Gd]DTPA-PEG-HCC-treated lymph nodes show a bright band along their edge. Twenty-four hours post-injection, mice were imaged using T1-weighed scans through their inguinal lymph nodes. Image (a.) is is the lymph node of a vehicle-treated mouse, whereas image (b.) is the lymph nodes from a [Gd]DTPA-PEG-HCC- treated mouse. Increased signal intensity can be visualized along the edge of the [Gd]DTPA-PEG-HCC- treated lymph node, however, no such signal intensity increase can be discerned in the vehicle-treated lymph node.

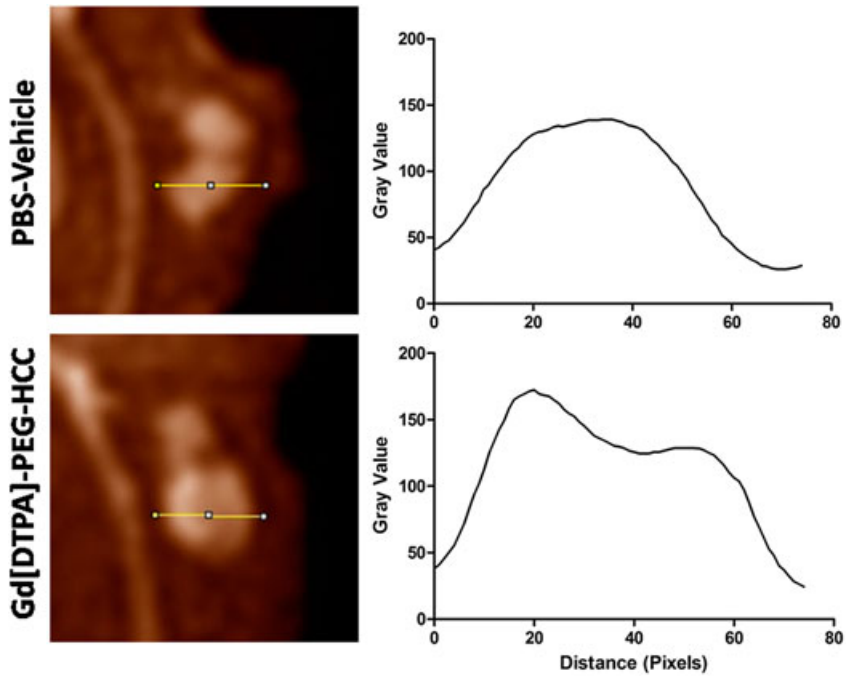

Figure 7. Plot profile through the lymph node shows increased signal intensity (SI) on the edge of the lymph node. An increase in SI can be seen along the edge of the lymph node treated with [Gd]DTPA-PEG-HCC on the bottom compared to the vehicle-treated lymph node shown on the top. Images were initially normalized to water phantom and then a Gaussian filter was applied to increase the contrast of the lymph nodes.

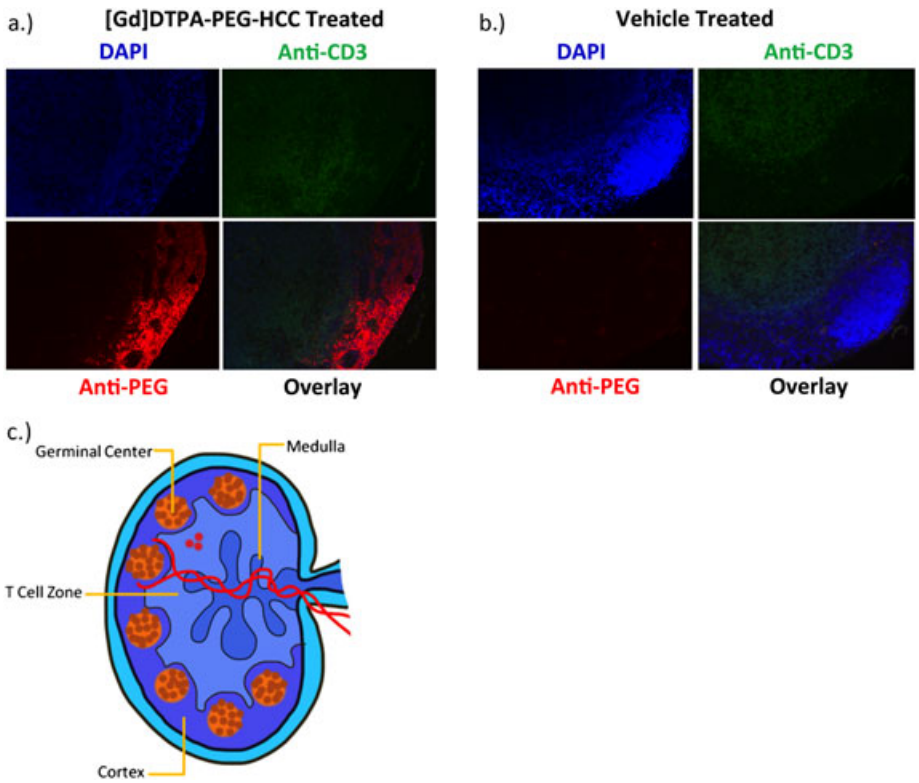

Figure 8. Accumulation of [Gd]DTPA-PEG-HCCs is seen in the lymph node cortex around the germination centers. [Gd]DTPA-PEG-HCCs (red) accumulate in the cortex, including the area surrounding germination centers within lymph nodes as shown in (a). This area is adjacent to the T-cell zone as evidenced by positive CD3 staining (green). Positive [Gd]DTPA-PEG-HCC staining is absent in images taken from vehicle treated lymph nodes as shown in (b). All images are 20X magnification. A schematic of the lymph node is shown in (c) to indicate relevant regions where positive [Gd]DTPA-PEG-HCC staining was observed.

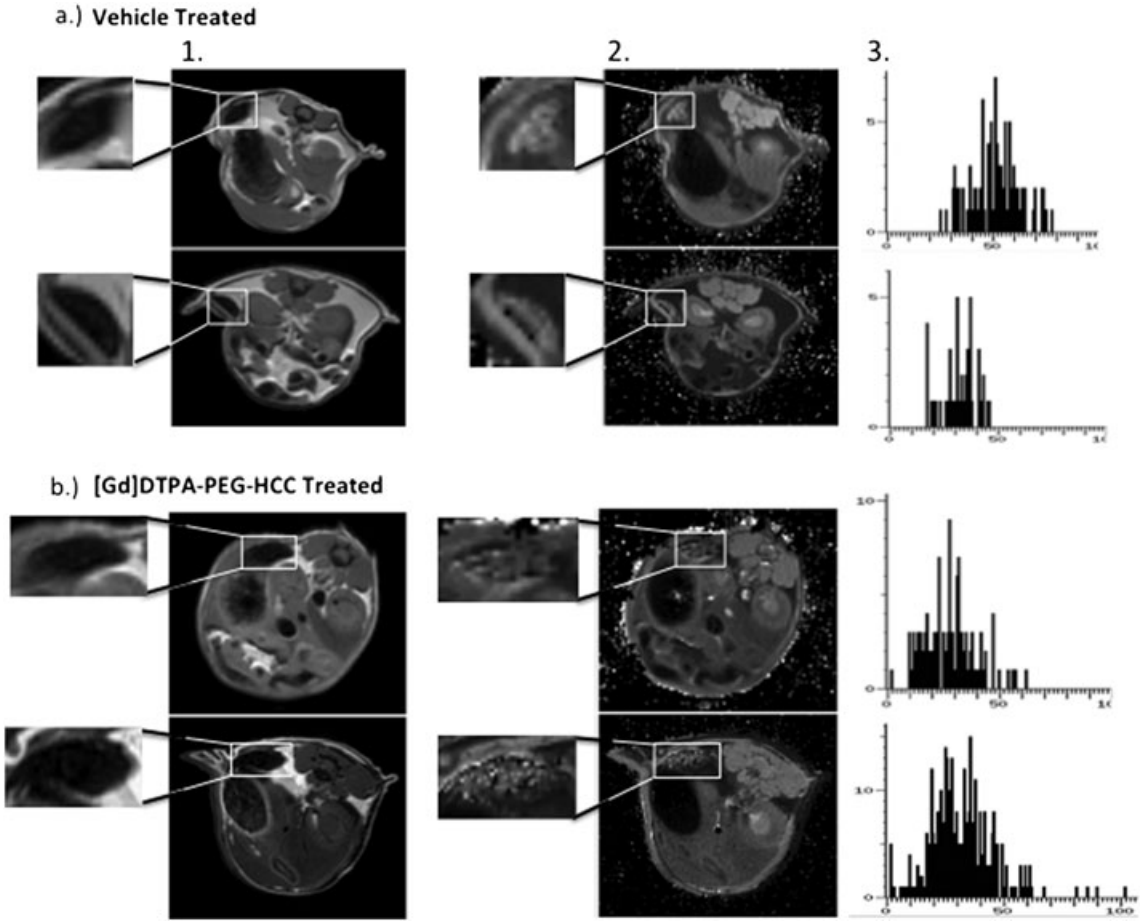

Figure 9. T_1 maps of the spleen demonstrate lower T_1 values in animals treated with [Gd]DTPA-PEG-HCC compared with saline. T_1 maps of [Gd]DTPA-PEG-HCC-treated mice show lower values in the spleens compared with those treated with saline. Twenty-four hours post-injection, mice were imaged using T_1-weighed scans through the spleens. Image (a) two mice treated with saline, (b) two mice treated with [Gd]DTPA-PEG-HCC. In column 1, anatomical scans are presented. In column 2, T_1 maps are presented. The insets are zoomed in views of the spleen for both sets of data. Column 3 is a histogram generated in PV 5.1 within a region of interest in the spleen only. Note that the T_1 values are shifted lower in the PEG-HCC-treated animals. Decreases in the T_1 can be visualized throughout the [Gd]DTPA-PEG-HCC-treated spleens although it is not uniform. The T_1 maps do not demonstrate nearly the degree of decreased T_1 values in the vehicle-treated spleens as shown in the histograms.

We then used flow cytometry to determine if the [Gd]DTPA-PEG-HCCs were accumulating within the T cell within the spleen.

PEG-HCCs accumulate in T cells of the spleen

Purified populations of T cells from the spleen (Fig. 10a) were assessed for the presence of PEG-HCC (Fig. 10b). Within each treatment group, intact and permeabilized T cells were both assessed to determine if cells are internalizing PEG-HCC instead of the nanomaterial simply binding to the cell surface. Figure 10c quantifies this difference and shows, within the PEG-HCC-treated group, a significantly greater PEG signal in the permeabilized cells. This shows that PEG-HCCs are internalized by T cells in the spleen. In conjunction with our data showing that [Gd]DTPA-PEG-HCCs can be imaged *in vivo* by MR, this demonstrates a great potential of [GD]DTPA-PEG-HCCs for T cell tracking.

DISCUSSION

Previous work done by Bitner *et al.* showed the effectiveness of PEG-HCCs in lowering oxidative stress *in vitro* and *in vivo* in a rat model of traumatic brain injury (9). The use of PEG-HCCs as a nanovector has also been demonstrated by loading them with drugs for delivery (10). This allows for a two-hit treatment model involving the drug that the PEG-HCCs are loaded with along with their radical scavenging potential. In the same capacity, PEG-HCCs have been shown to be targetable with the non-covalent addition of antibodies to the sidewalls of the nanoparticle (10).

We identified several new facets of [Gd]DTPA-PEG-HCCs in this study. These nanoantioxidants are (i) immunomodulatory in that they can suppress recall immune response; (ii) accumulate within lymph nodes in areas surrounding the germinal centers, (iii) are internalized by splenic T cells; and (iv) can be visualized *in vivo* via MRI by conjugation to a T_1-contrast agent [GD]DTPA.

However, there are several challenges to being able to visualize lymph nodes. First, MRI slice selection is a challenge as a result of the small size of murine lymph nodes. Second, their positioning within the fat pads makes them candidates for susceptibility artifacts. Finally, as we are imaging live animals, the breathing motion, paired with the small size of the lymphoid organ we are attempting to visualize, add to the difficulty of acquiring images free of motion artifacts. We were able to visualize the general location of the [Gd]DTPA-PEG-HCCs in the

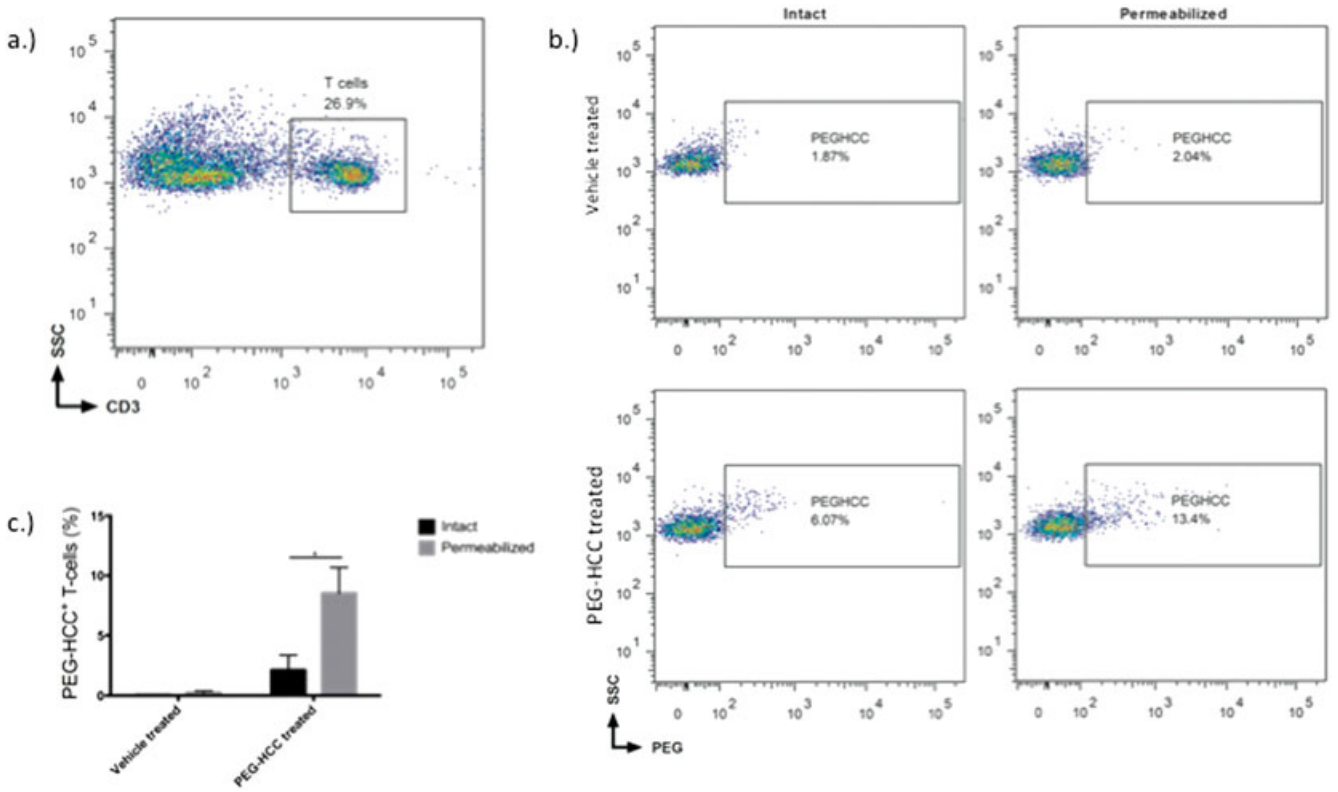

Figure 10. Splenic T cells take up PEG-HCCs. As shown in (a), the T cell surface marker CD3 was used to isolate a purified population of T cells from vehicle and PEG-HCC treated animals. These T cells were then assessed for the presence of PEG-HCCs as shown in (b) Among PEG-HCC-treated samples, permeabilized samples had significantly higher PEG positive cells than what was observed in intact samples. $n = 3$ per group. $^*p < 0.05$.

lymph nodes and observe that their localization coincides with the cortex surrounding the germinal centers. The spleen, on the other hand, demonstrated lower T_1 values as shown by T_1 mapping after treatment with [Gd]DTPA-PEG-HCCs. As we see that PEG-HCC treatment has an effect on the recall response, and we have shown that PEG-HCCs are internalized by splenic T-cells, we can conclude that PEG-HCCs and [Gd]DTPA-PEG-HCCs are internalized and can modulate the recall memory response.

This discovery of T cell uptake and modulation of the recall immune response by PEG-HCCs is an additional feature of these nanoantioxidants. Our findings give impetus to the possibility of utilizing PEG-HCCs (and their modified forms) in the treatment of inflammatory diseases in which oxidative stress is both an initiating and propagating factor. With this in mind, [Gd]DTPA-PEG-HCCs will not only be able to modulate the T cell response, but we will also have the ability to track whether the nanoantioxidants are tracking to and staying at sites where they will be most effective. As a result, it is of the utmost importance to continue further characterization of this nanoantioxidant in the treatment, and possibly the prevention, of human inflammatory diseases.

ACKNOWLEDGEMENTS

This project was supported by a grant award by NIH/NIDDK (R21DK093802) (RGP). D.M.G. was funded by a Howard Hughes Medical Institute Gilliam Fellowship for Advanced Study. The work at Rice University was funded by the Mission Connect Mild Traumatic Brain Injury consortium, funded by the Department of Defense (W81XWH-08-2-0143).This project was also supported by the Pathology and Histology Core at Baylor College of Medicine with funding from the NIH (NCI P30-CA125123) and the expert assistance of Michael Ittmann, MD Ph.D.

REFERENCES

1. Federico A, Cardaioli E, Da Pozzo P, Formichi P, Gallus GN, Radi E. Mitochondria, oxidative stress and neurodegeneration. J. Neurol. Sci. 2012; 322: 254–262.
2. Behl C. Alzheimer's disease and oxidative stress: implications for novel therapeutic approaches. Prog. Neurobiol. 1999; 57: 301–323.
3. Rego AC, Oliveira CR. Mitochondrial dysfunction and reactive oxygen species in excitotoxicity and apoptosis: Implications for the pathogenesis of neurodegenerative diseases. Neurochem. Res. 2003; 28: 1563–1574.
4. Lee D-H, Gold R, Linker RA. Mechanisms of oxidative damage in multiple sclerosis and neurodegenerative diseases: Therapeutic modulation via fumaric acid esters. Int. J. Mol. Sci. 2012; 13: 11783–11803.
5. Linseman DA. Targeting oxidative stress for neuroprotection. Antioxid. Redox Signal. 2009; 11: 421–424.
6. Onyango IG, Khan SM. Oxidative stress, mitochondrial dysfunction, and stress signaling in Alzheimer's disease. Curr. Alzheimer Res. 2006; 3: 339–349.
7. Kowaltowski AJ, Vercesi AE. Mitochondrial damage induced by conditions of oxidative stress. Free Radic. Biol. Med. 1999; 26: 463–471.
8. Lucente-Schultz RM, Moore VC, Leonard AD, Price BK, Kosynkin DV, Lu M, Partha R, Conyers JL, Tour JM. Antioxidant single-walled carbon nanotubes. J. Am. Chem. Soc. 2009; 131: 3934–3941.
9. Bitner BR, Marcano DC, Berlin JM, Fabian RH, Cherian L, Culver JC, Dickinson ME, Robertson CS, Pautler RG, Kent TA, Tour JM. Antioxidant carbon particles improve cerebrovascular dysfunction following traumatic brain injury. ACS Nano 2012; 6: 8007–8014.
10. Berlin JM, Leonard AD, Pham TT, Sano D, Marcano DC, Yan S, Fiorentino S, Milas ZL, Kosynkin DV, Price BK, Lucente-Schultz RM, Wen X, Raso MG, Craig SL, Tran HT, Myers JN, Tour JM. Effective drug delivery, in vitro and

in vivo, by carbon-based nanovectors noncovalently loaded with unmodified paclitaxel. ACS Nano 2010; 4: 4621–4636.
11. Srinivas M, Morel PA, Ernst LA, Laidlaw DH, Ahrens ET. Fluorine-19 MRI for visualization and quantification of cell migration in a diabetes model. Magn. Reson. Med. Off. J. Soc. Magn. Reson. Med. Soc. Magn. Reson. Med. 2007; 58: 725–734.
12. Beer AJ, Holzapfel K, Neudorfer J, Piontek G, Settles M, Krönig H, Peschel C, Schlegel J, Rummeny EJ, Bernhard H. Visualization of antigen-specific human cytotoxic T lymphocytes labeled with superparamagnetic iron-oxide particles. Eur. Radiol. 2008; 18: 1087–1095.
13. Liu L, Ye Q, Wu Y, Hsieh W-Y, Chen C-L, Shen H-H, Wang S-J, Zhang H, Hitchens TK, Ho C. Tracking T-cells in vivo with a new nano-sized MRI contrast agent. Nanomedicine Nanotechnol. Biol. Med. 2012; 8: 1345–1354.
14. Srinivas M, Heerschap A, Ahrens ET, Figdor CG, de Vries IJM. 19F MRI for quantitative in vivo cell tracking. Trends Biotechnol. 2010; 28: 363–370.
15. Beeton C, Pennington MW, Wulff H, Singh S, Nugent D, Crossley G, Khaytin I, Calabresi PA, Chen CY, Gutman GA, Chandy KG. Targeting effector memory T cells with a selective peptide inhibitor of Kv1.3 channels for therapy of autoimmune diseases. Mol. Pharmacol. 2005; 67: 1369–1381.
16. Karfeld-Sulzer LS, Waters EA, Kohlmeir EK, Kissler H, Zhang X, Kaufman DB, Barron AE, Meade TJ. Protein polymer MRI contrast agents: Longitudinal analysis of biomaterials in vivo. Magn. Reson. Med. Off. J. Soc. Magn. Reson. Med. Soc. Magn. Reson. Med. 2011; 65: 220–228.